



RESEARCH ARTICLE

10.1029/2021GC010212

Changes in Magnetic Properties of Magnetite Nanoparticles
Upon Microbial Iron Reduction

Key Points:

- Microbially reduced magnetite nanoparticles (NPs) have larger lattice parameters compared to pristine ones
- Microbial reduction of magnetite NPs leads to a softer magnetism and increasing magnetic susceptibility
- Partially oxidized magnetite is resistant to bioreduction

Supporting Information:

Supporting Information may be found in the online version of this article.

Correspondence to:

Z. Zhu and D. Liu,
zhumin@cug.edu.cn;
liudeng@cug.edu.cn

Citation:

Wang, P., Shi, T., Mehta, N., Yang, S., Wang, H., Liu, D., & Zhu, Z. (2022). Changes in magnetic properties of magnetite nanoparticles upon microbial iron reduction. *Geochemistry, Geophysics, Geosystems*, 23, e2021GC010212. <https://doi.org/10.1029/2021GC010212>

Received 13 OCT 2021

Accepted 11 FEB 2022

Pengcong Wang¹ , Taiheng Shi¹ , Neha Mehta² , Shanshan Yang^{3,4} , Hongmei Wang^{3,4} , Deng Liu^{3,4} , and Zongmin Zhu^{1,3}

¹School of Earth Sciences, Hubei Key Laboratory of Critical Zone Evolution, China University of Geosciences, Wuhan, China, ²Sorbonne Université, Institut de Minéralogie, de Physique des Matériaux et de Cosmochimie, IMPMC, Paris, France, ³State Key Laboratory of Biogeology and Environmental Geology, China University of Geosciences, Wuhan, China, ⁴School of Environmental Studies, China University of Geosciences, Wuhan, China

Abstract The magnetic signals of magnetite nanoparticles (NPs) preserved in rocks, soils, and sediments are effective index for paleoenvironmental reconstruction. It has been demonstrated that magnetite NPs can serve as a terminal electron sink for the microbial respiration (i.e., microbial iron reduction). The magnetic properties of magnetite NPs may be altered by microbial iron reduction, which is a critical but often overlooked process in paleomagnetism. In this study, three magnetite NPs with different particle sizes were reduced by a dissimilatory iron-reducing bacterium (*Shewanella oneidensis* MR-1) under a non-growth condition mimicking that of the early Earth and modern oligotrophic environment. The changes in magnetic, chemical as well as crystallographic properties of the magnetite NPs during the microbial reduction process were examined. Our results showed that the bioreduction rate of magnetite NPs was mainly controlled by their particle size and redox state. In addition, the microbial iron reduction could affect both the crystallographic and magnetic properties of three types of magnetite NPs used herein. After bioreduction, the crystal lattice parameters and magnetic susceptibility of the magnetite NPs increased, while their remanence recording capability and coercivity decreased (i.e., “softer” magnetism). Furthermore, bioreduced magnetite NPs had a larger remanence loss near the Verwey transition region with low-temperature magnetic analysis. These results indicate that the microbial reduction of magnetite NPs deserves attention when sedimentary magnetites are used in paleoenvironment reconstruction.

Plain Language Summary Natural magnetite nanoparticles (NPs) in rocks, soils, and sediments can record the paleoenvironment information when they were formed. Of note, in anaerobic post depositional environments, magnetite-bound Fe (III) can act as an electron sink for iron-reducing microorganisms. This microbe-magnetite interaction has the potential to affect magnetic properties of magnetite NPs. In doing so, the original paleoenvironment information carried by magnetite NPs might also be rewritten. Therefore, to extract the paleoenvironment information from sedimentary magnetite NPs, we should understand the impact of bioreduction on natural magnetite NPs before burial diagenesis. Three magnetite NPs with different particle sizes were exposed to a typical dissimilatory iron-reducing bacterium (*Shewanella oneidensis* MR-1) under a non-growth condition mimicking that of the early Earth and modern oligotrophic environments. We examined the changes in magnetic, chemical as well as crystallographic properties of the magnetite NPs during the bioreduction process. Our study found that the bioreduction rate of magnetite NPs was mainly controlled by their particle size and redox state. After bioreduction, the magnetism of magnetite NPs became “softer.” These results indicate that the microbial reduction of magnetite NPs deserves attention when natural magnetites are used in paleoenvironment reconstruction.

1. Introduction

Natural magnetite nanoparticles (NPs) are important iron oxides in the surficial Earth system, and widely used as a paleoenvironmental indicator (e.g., Chang et al., 2016; Faivre & Schuler, 2008; J. H. Li et al., 2009; J. H. Li, Benzerara, et al., 2013; Liu et al., 2012; Maher, 2011; Zhu et al., 2012). The natural magnetite NPs have multiple origins, including volcano eruption, magmatic crystallization, rock weathering and pedogenesis, and biologically controlled or biologically induced mineralization (Byrne et al., 2015; J. H. Li et al., 2020, 2021; Liu et al., 2012; Zhou et al., 2019). Various magnetic properties that reveal the concentration, domain state, and crystallinity of magnetite NPs are closely associated with the past environmental changes (Liu et al., 2012). For

© 2022. The Authors.

This is an open access article under the terms of the Creative Commons Attribution-NonCommercial-NoDerivs License, which permits use and distribution in any medium, provided the original work is properly cited, the use is non-commercial and no modifications or adaptations are made.

instance, variations in the concentrations of magnetite and maghemite NPs mainly control the magnetic susceptibility in loess and paleosol from central China (An & Porter, 1997; Ding et al., 2002; Heller & Liu, 1986; Liu et al., 2005, 2012). Based on these findings, the regional paleoenvironment changes over the last 2.5 million years have been successfully reconstructed (Liu et al., 2005, 2012). In addition, the biogenic magnetite NPs with unique morphology and domain state in marine sediments have been proved to be related to the changes of sedimentation rates and paleoproductivity during Quaternary glacial-interglacial cycles (Bazylinski & Moskowitz, 1997; Chang et al., 2016, 2018; Faivre & Schuler, 2008; Y. L. Li et al., 2009; Liu et al., 2012).

The unit cell of magnetite contains eight Fe^{2+} and eight Fe^{3+} octahedrally coordinated ions (B site), which are coupled in antiparallel magnetic orientation to eight Fe^{3+} tetrahedral coordinated ions (A site) (Byrne et al., 2015; Jiang et al., 2016). The strong magnetization of magnetite can be ascribed to the net magnetization of octahedrally coordinated Fe^{2+} on B sites, owing to the fact that the magnetic spin directions of Fe^{3+} on B sites are antiparallel to those on A sites so that they completely cancel each other (Byrne et al., 2015; Gorski & Scherer, 2010; Jiang et al., 2016). In this regard, the balance between Fe^{2+} and Fe^{3+} in the B sites or redox state controls the magnetic behavior of the magnetite NPs (Byrne et al., 2016).

Noticeably, iron oxides often undergo 100–300 times of Fe(II)–Fe(III) transition before burial (Canfield et al., 1993). Therefore, the magnetic properties of magnetite NPs might be altered during the reduction or oxidation processes that commonly occur during deposition (Liu et al., 2012; Y. L. Li, et al., 2013; Zhou et al., 2019). For example, oxidized magnetite NPs with a $\text{Fe}^{2+}/\text{Total Fe}$ ($\text{Fe}^{2+}/\text{Fe}_T$) ratio lower than 33% exhibit smaller lattice parameters, lower magnetic susceptibility, and higher coercivity than the perfect stoichiometric magnetite NPs (i.e., $\text{Fe}^{2+}/\text{Fe}_T = 33\%$; Byrne et al., 2015, 2016; Gorski & Scherer, 2010; Y. L. Li et al., 2009; Radon et al., 2020; Zhou et al., 2019). By employing a low-temperature magnetic analysis, Özdemir and Dunlop (2010) further reported a broader Verwey transition region and lower remanence loss in partially oxidized magnetite NPs. Given the presence of structurally coordinated Fe(III), magnetite NPs can also function as an electron sink or even “biogeochemical battery” for microorganisms, especially in anaerobic or fluctuating redox regimes (Byrne et al., 2015, 2016). Besides modern ecosystems, it has been thought that microbial iron reduction is likely one of the earliest forms of microbial respiration due to the lack of other electron acceptors such as oxygen, nitrate, and sulphate (Vargas et al., 1998; Walker, 1987; Walker & Brimblecombe, 1985; Wiechert, 2002). In this reduction process, magnetite NPs could carry excess Fe^{2+} (i.e., $\text{Fe}^{2+}/\text{Fe}_T > 33\%$; Byrne et al., 2015, 2016; Dong et al., 2000; Gorski & Scherer, 2010; Kukkadapu et al., 2005; Y. L. Li et al., 2009; Zhou et al., 2019). However, the changes in mineralogical and magnetic properties of magnetite NPs during microbial iron reduction are not well understood.

In this study, we examined the reduction process of magnetite NPs by *Shewanella oneidensis* MR-1, a typical dissimilatory iron-reducing bacterium (DIRB). Our results indicated that both mineralogical and magnetic properties of magnetite can be altered upon microbial iron reduction, and that multiple magnetic parameters are indicative of $\text{Fe}^{2+}/\text{Fe}_T$ ratio of magnetite NPs.

2. Materials and Methods

2.1. Source of Magnetite NPs

Three magnetite NPs with different particle sizes were used for bioreduction experiments, including a commercial magnetite sample and two laboratory-synthesized samples. The commercial magnetite was purchased from Sigma-Aldrich (CAS No. 1317-61-9; abbreviated as SM). In addition, a hydrothermal method and a coprecipitation approach were utilized to prepare laboratory-synthesized magnetite NPs. Specifically, for the hydrothermal synthesized magnetite NPs (HM), 49 g $\text{FeSO}_4 \cdot 7\text{H}_2\text{O}$ were dissolved in 190 mL of deionized water (DI H_2O) with heating and stirring (90°C, 50 rpm), and 80 mL mixed solution of NaOH (18.8%, w/v) and KNO_3 (2.5%, w/v) was added dropwise into aforementioned Fe(II) solution (Lei et al., 2017). After aging for 60 min, the HM was collected by centrifugation and washed with DI H_2O three times. For preparation of the coprecipitation-synthesized magnetite NPs (CM), 5.97 g $\text{FeCl}_2 \cdot 4\text{H}_2\text{O}$ and 16.23 g $\text{FeCl}_3 \cdot 6\text{H}_2\text{O}$ were dissolved in 200 mL of DI H_2O with heating and stirring (60°C, 50 rpm), and 200 mL $\text{NH}_3 \cdot \text{H}_2\text{O}$ (25%, v/v) was added drop by drop (Ghosh et al., 2011). The resulting CM particles were obtained by centrifugation and further washed with DI H_2O . To avoid air oxidation, these three magnetite NPs were kept in an anaerobic chamber (filled with 98% N_2 and 2% H_2 , Coy Laboratory Products, Michigan, USA) for future use (the SM sample is not anaerobic storage during transportation to the laboratory).

2.2. Microbial Iron Reduction Experiments

Cells of *S. oneidensis* MR-1 were aerobically cultured in a Luria-Bertani (LB) medium. Specifically, cells from the exponential phase (after 12 h cultivation) were harvested through centrifugation and washed three times in sterile NaCl solution (0.9%, w/v) to thoroughly remove the residual medium. Bacterial reduction experiments were anaerobically performed in 15 mL serum bottles with 30 mM PIPES (piperazine-1,4-bisethanesulfonic acid) buffer (pH ~ 7.0), 10 mM lactate (as the sole electron donor), 48 mM magnetite NPs (final conc. ~ 11 g/L), and a cell concentration of ~10⁸ cells/mL. It has been demonstrated that DIRB can utilize exogenous quinones as electron shuttles to facilitate the electron transfer between microbial cells and Fe(III) minerals (Lovley et al., 1996). In order to expand the magnetic measurement range toward to higher bioreduction degree, the well-studied electron shuttle anthraquinone-2,6-disulfonate (AQDS) was added into our biosystems to achieve a final concentration of 0.1 mM. All experiments were conducted in duplicates, and sterile controls were set up simultaneously.

2.3. Chemical Analysis

The supernatant and residual solid phases were separated at selected time points by a neodymium magnet. Prior to chemical analyses, the supernatant was filtered through 0.22 μm filter. The Fe concentrations in the supernatant were determined using an inductively coupled plasma mass spectrometer (Agilent 7900). The Fe²⁺ and total Fe concentrations of the pristine and bioreduced magnetite NPs were measured using the phenanthroline method after dissolved anaerobically by a 6 M HCl (Tamura et al., 1974).

2.4. Mineral Characterization

The pristine and bioreduced magnetite NPs that were sampled at 5 and 14 days were selected for mineral characterization, including X-ray diffraction (XRD), transmission electron microscope (TEM), and Fourier transform infrared (FTIR). The XRD patterns of the magnetite were collected using X-ray diffractometer (Rigaku MiniFlex 600) with a copper tube Cu Kα (λ = 0.15406 nm), a tube voltage of 40 kV, and a current of 15 mA, using a D/teX Ultra silicon strip detector. The TEM images were obtained using a transmission electron microscope (STEM TITAN 80–300) after placing the magnetite NPs re-dispersed in ethanol into the copper grid with a carbon film and dried at ambient temperature. The FTIR spectra were recorded for each magnetite at room temperature using spectrophotometer FTIR (Nicolet 6700/8700). Measurements of samples were conducted in the transmission mode in the mid-infrared range of 4000–4400 cm⁻¹ using KBr pellets.

2.5. Magnetism Analysis

The changes of magnetic susceptibility (χ) and frequency-dependent susceptibility (χ_{fd}%) of the magnetite NPs during experiment processes were monitored directly in serum bottles with a kappabridge MFK1-FA (AGICO, Brno). Magnetic susceptibility at low (χ_{lf}, 976 Hz) and high (χ_{hf}, 15,616 Hz) frequencies were measured at 200 Am⁻¹ field intensity. The χ_{lf} values were calculated as a mass-specific susceptibility (χ) in 10⁻⁸m³kg⁻¹. The χ_{fd}% values were then calculated and expressed as a percentage χ_{fd}% = (χ_{lf} - χ_{hf})/χ_{lf} × 100% (Zhu et al., 2012).

The hysteresis loops (at room temperature) and the zero-field warming (ZFC, 10–300 K) and field warming curves (FC, 10–300 K) of low temperature saturation isothermal remanent magnetization (LT-SIRM) of the pristine and bioreduced magnetite NPs were determined by a superconducting quantum interference device (SQUID) magnetometer (Quantum Design MPMS-3). The dried magnetite NPs were gently grounded by an agate mortar, mixed with epoxy resin (1%, w/v), and fully stirred to eliminate the influence of magnetostatic interactions. All of the above operations were conducted in the anaerobic chamber to avoid possible oxidation. The ratio of saturation remanence to saturation magnetization (M_{rs}/M_s), indicating the remanence recording capacity of magnetite (Dunlop, 2002a, 2002b; Liu et al., 2012), and coercivity (B_c) were determined by the room temperature hysteresis loops. The behavior of a LT-SIRM acquired in a 2.5 T field at 10 K after cooling the sample from 300 to 10 K in zero field (ZFC) and in a 2.5 T field (FC) was monitored upon warming from 10 to 300 K in 5 K steps (Kosterov, 2003; Özdemir & Dunlop, 2010).

Table 1

Chemical, Mineralogical, and Magnetic Parameters for Solutions and Magnetite Nanoparticles Before and After Bioreduction Experiments

Culturing days	SM			HM			CM		
	0 days	5 days	14 days	0 days	5 days	14 days	0 days	5 days	14 days
Supernatant pH	7.00 ± 0.05	7.00 ± 0.07	6.93 ± 0.09	7.00 ± 0.10	7.12 ± 0.12	7.05 ± 0.07	7.00 ± 0.12	7.09 ± 0.03	7.12 ± 0.06
Fe ²⁺ /Total Fe _T (Chemistry)	0.30 ± 0.01	0.34 ± 0.00	0.37 ± 0.03	0.33 ± 0.02	0.35 ± 0.00	0.37 ± 0.03	0.33 ± 0.04	0.37 ± 0.00	0.39 ± 0.01
Soluble Fe (mM)	~0	0.59 ± 0.08	0.53 ± 0.09	~0	0.62 ± 0.14	0.69 ± 0.04	~0	0.75 ± 0.08	0.99 ± 0.07
Lattice constant (a ₀ = b ₀ = c ₀ , Å)	8.3806	–	8.3832	8.4014	–	8.4069	8.4067	–	8.4104
Size (nm)	120 ± 25.0	–	122 ± 38.5	79.7 ± 16.2	–	69.3 ± 16.6	12.5 ± 3.6	–	11.5 ± 2.5
Δχ ^a (%)	0	13.8 ± 1.60	19.7 ± 0.92	0	5.09 ± 0.74	9.91 ± 1.41	0	19.1 ± 1.05	22.9 ± 1.14
M _r /M _s (10 ⁻¹²)	10.2 ± 0.06	9.62 ± 0.25	8.78 ± 0.25	18.1 ± 0.52	16.8 ± 0.83	15.7 ± 0.83	0.34 ± 0.04	0.31 ± 0.10	0.32 ± 0.00
B _c (A m ⁻¹)	9.25 ± 0.07	9.00 ± 0.28	8.20 ± 0.28	13.9 ± 0.14	13.7 ± 0.42	13.5 ± 0.14	0.25 ± 0.07	0.25 ± 0.07	0.20 ± 0.00
LT-SIRM loss in ZFC ^b (%)	18.1 ± 0.93	21.0 ± 0.48	24.5 ± 1.11	59.1 ± 3.36	61.1 ± 0.39	62.3 ± 0.50	–	–	–
LT-SIRM loss in FC ^c (%)	19.3 ± 0.74	21.0 ± 0.31	21.8 ± 0.98	58.8 ± 2.03	59.5 ± 0.00	59.7 ± 0.52	–	–	–

Note. The data errors represented the values range of duplicate experiments.

^aThe change of magnetic susceptibility (χ) of magnetite after bio-reduction. ^bExpressed by the peak area of the first derivative curve of ZFC to temperature. ^cExpressed by the peak area of the first derivative curve of FC to temperature.

3. Results

3.1. Chemical Analysis of Supernatant and Solid Phase

During the incubation, the pH of the supernatant remained within the circum-neutral range for each bio-treatment (Table 1). With increasing culture time, the Fe²⁺/Fe_T ratios of the magnetite NPs and the soluble Fe concentrations in the supernatant increased gradually within 10 days and then leveled off with time (Figure 1). Among the tested magnetites, bio-reduced CM had the highest values of Fe²⁺/Fe_T ratios and soluble Fe (Table 1). At the end of experiments (day 14), the concentrations of soluble Fe were found to range from 0.53 to 0.99 mM (Table 1), corresponding to the solubility fractions ranging from 0.11% to 0.21%. These data suggest that the reductive dissolution of magnetite NPs was a negligible process.

3.2. Comparison of Pristine and Bio-reduced Magnetite NPs

The XRD patterns of the pristine and bio-reduced magnetite are shown in Figure S1 in Supporting Information S1, and the precise lattice constants estimated by extrapolating the Bragg angle to 90° are shown in Table 1. Except for minor maghemite detected in the pristine SM, no other secondary mineral was found before and after microbial reduction of the magnetite NPs (Figure S1 in Supporting Information S1). The nano-size characteristics of the three magnetite NPs caused XRD peaks to be weakened and broadened, and this phenomenon was intensified after microbial reduction (Figure S1 in Supporting Information S1). For the pristine samples, the lattice constants of SM (8.3806 Å) were smaller than that of the theoretical magnetite (8.3967 Å). In contrast, the lattice constants of HM (8.4014 Å) and CM (8.4067 Å) were similar to that of the theoretical magnetite (Table 1). After microbial reduction, the lattice constants of the three magnetite NPs increased slightly (Table 1), and the maghemite peaks in SM disappeared (Figure S1 in Supporting Information S1).

The TEM results showed the crystallographic differences between pristine and bio-reduced magnetite NPs (Figure 2). For SM, there was no significant

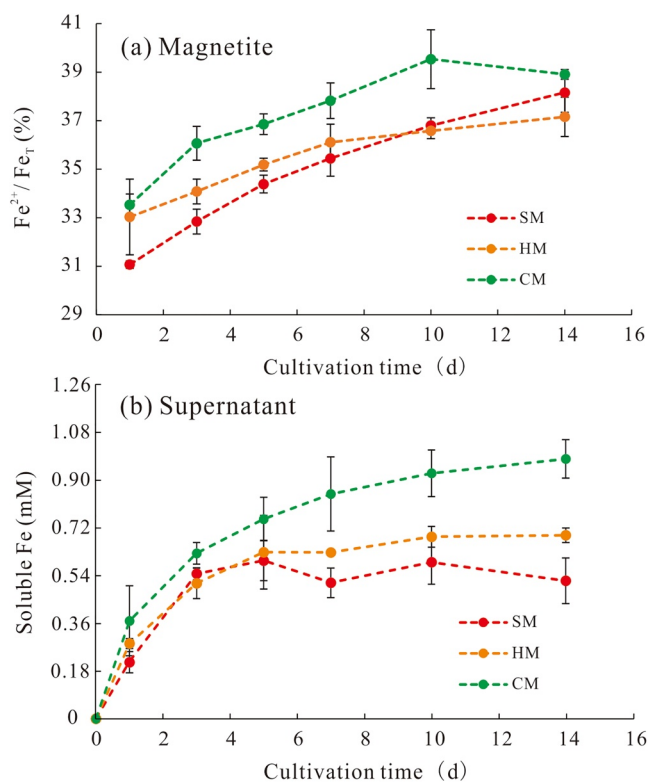


Figure 1. (a) The variations of Fe²⁺/Fe_T ratio in magnetite nanoparticles and (b) the soluble Fe in supernatant with culture time. Error bar represented the values range of duplicate experiments.

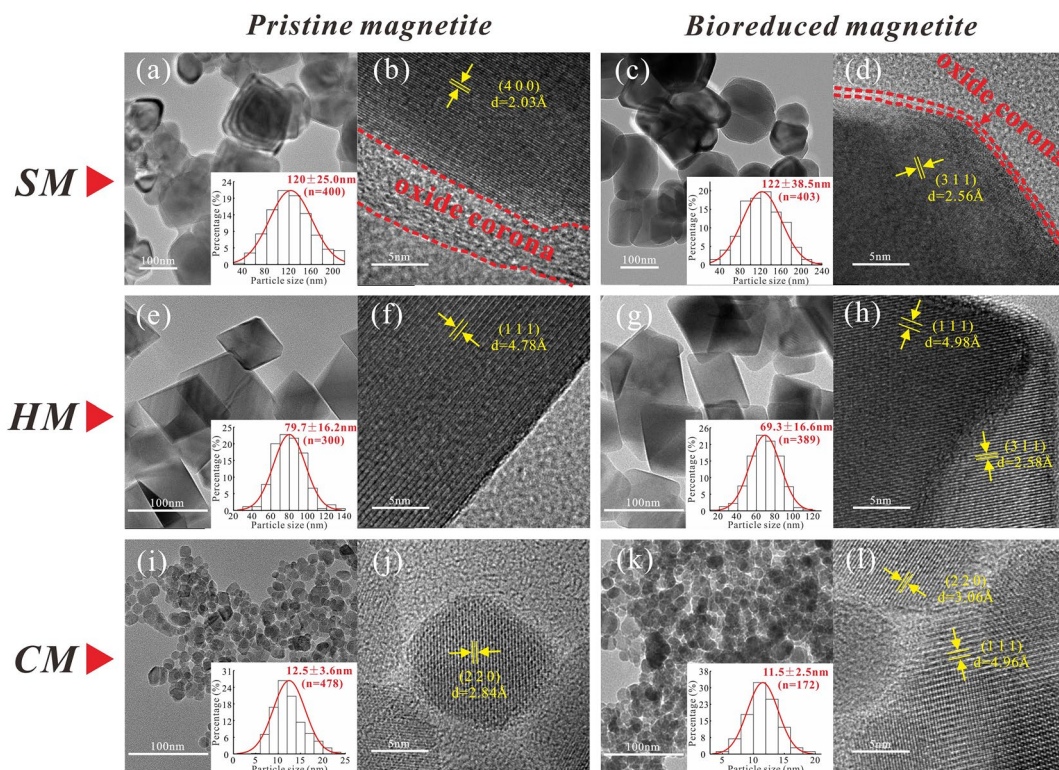


Figure 2. TEM images and particle size distributions of (a–d) SM, (e–h) HM, and (i–l) CM before and after bioreduction.

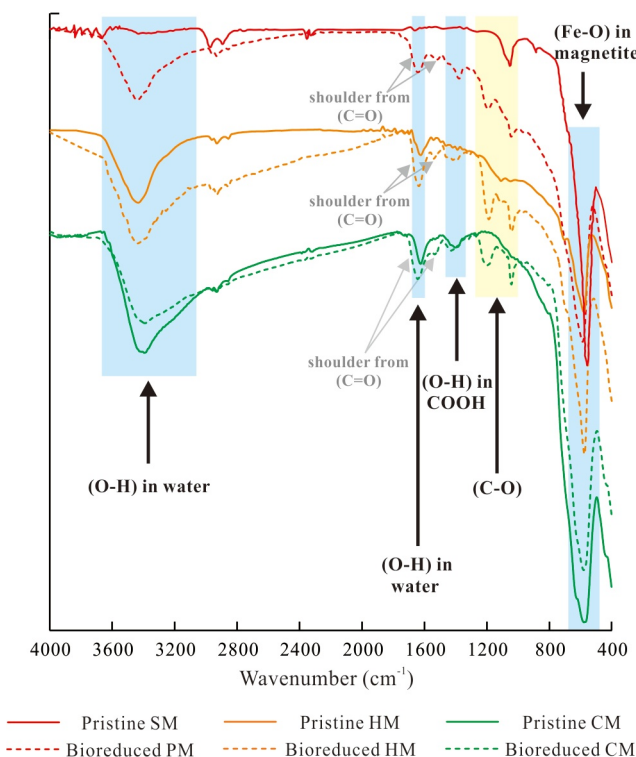


Figure 3. FTIR spectra of the pristine and bioreduced magnetite NPs by MR-1.

change in particle size before and after bioreduction (120 ± 25.0 nm vs. 122 ± 38.5 nm) (Figures 2a and 2c). High-resolution TEM (HRTEM) images further revealed that the interplanar spacing of pristine SM ($d_{400} = 2.03$ Å) is smaller than that of the perfect stoichiometric magnetite ($d_{400} = 2.10$ Å, PDF ID: 99–0073), but the interplanar spacing of bioreduced SM ($d_{311} = 2.56$ Å) is larger than that of perfect stoichiometric magnetite ($d_{311} = 2.53$ Å, PDF ID: 99–0073) (Figures 2b and 2d). In addition, HRTEM observed an amorphous oxide corona surrounding the pristine SM particles (Figure 2b). It is noted that this corona-like structure became thinner upon bioreduction (Figure 2d). For HM, an octahedral crystal was observed at low magnification (Figures 2e and 2g). After microbial reduction, the particle size of HM decreased slightly from 79.7 ± 16.2 to 69.3 ± 16.6 nm. Meanwhile, HRTEM showed that the interplanar spacing (d_{311}) of HM increased from 4.78 to 4.98 Å after bioreduction (Figures 2f and 2h). The CM is mainly irregular spherical at low magnification TEM (Figures 2i and 2k). After bioreduction, the particle size of CM decreased from 12.5 ± 3.6 to 11.5 ± 2.5 nm, while the interplanar spacing (d_{220}) increased from 2.84 to 3.06 Å (Figures 2j and 2l).

The FTIR results showed that after microbial reduction, the OH stretching vibration of the water molecules at ~ 3354 cm^{-1} became much clearer (Figure 3). New peaks emerged at 1040, 1188, and 1390 cm^{-1} , which are ascribed to polysaccharide (C–O), phenol (C–O), and carboxyl (OH), respectively (Byrne et al., 2015; Tang et al., 2013). Moreover, the peak broadening and shoulder peaks around the peak of O–H (water, ~ 1630 cm^{-1}) are considered to be caused by C=O in carboxyl groups (Radon et al., 2020).

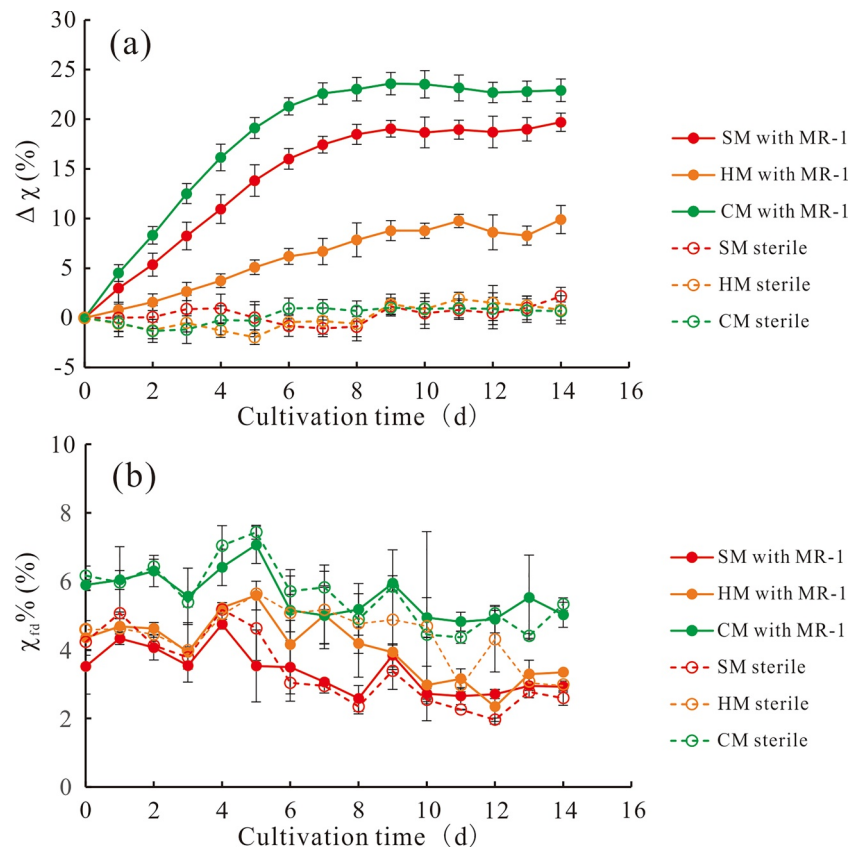


Figure 4. (a) The variations of magnetic susceptibility (χ) and (b) frequency-dependent susceptibility (χ_{fd}) of magnetite nanoparticles during culture.

3.3. Magnetic Parameters of Magnetite NPs Before and After Bioreduction

The changes of χ and χ_{fd} of magnetite NPs during the bioreduction were shown in Figure 4. The ZFC and FC of LT-SIRM for the magnetite NPs were shown in Figure 5, and their LT-SIRM loss near Verwey transition region were shown in Table 1. No increases in χ values were observed in sterile groups (Figure 4a). In the bioreduction experiments, χ increased rapidly during the first 10 days, and kept stable thereafter (Figure 4a). These trends are similar to those of $\text{Fe}^{2+}/\text{Fe}_T$ ratio described earlier (Figure 1a). At the end of the experiments (day 14), the χ values of SM, HM, and CM increased by $19.7\% \pm 0.92\%$, $9.91\% \pm 1.41\%$, and $22.9\% \pm 1.14\%$, respectively (Figures 4a and Table 1). The χ_{fd} values of SM and HM ($\sim 4\%$) were lower than those of CM ($\sim 6\%$) (Figure 4b). Comparatively, the ZFC and FC of HM had a narrower Verwey transition region (Figures 5c and 5d) and a higher LT-SIRM loss (Table 1) than that of SM. In addition, there was no obvious Verwey transition region in ZFC and FC found for CM (Figures 5e and 5f).

The relationships between magnetic parameters (including the changes of χ ($\Delta\chi$, normalized by the initial values), M_{rs}/M_s , B_c , and LT-SIRM loss near Verwey transition region) and $\text{Fe}^{2+}/\text{Fe}_T$ ratios were shown in Figure 6. The $\Delta\chi$ values of the three magnetite NPs increased linearly with the increasing $\text{Fe}^{2+}/\text{Fe}_T$ ratios (Figure 6a). The steeper slope between $\Delta\chi$ and $\text{Fe}^{2+}/\text{Fe}_T$ found for CM than those for SM and HM suggested that χ values of CM is more sensitive to the $\text{Fe}^{2+}/\text{Fe}_T$ ratios. The M_{rs}/M_s values and B_c of HM were higher than those of SM (Figures 6b and 6c). Moreover, both M_{rs}/M_s values and B_c of SM and HM were inversely proportional to $\text{Fe}^{2+}/\text{Fe}_T$ ratios (Figures 6b and 6c and Table 1). While, the M_{rs}/M_s values and B_c of CM were much lower than those of SM and HM (Table 1). In addition, for SM and HM, the LT-SIRM loss near Verwey transition region also increased linearly with the increase of the $\text{Fe}^{2+}/\text{Fe}_T$ ratios ($R^2 = 0.98$, Figures 6d and Table 1).

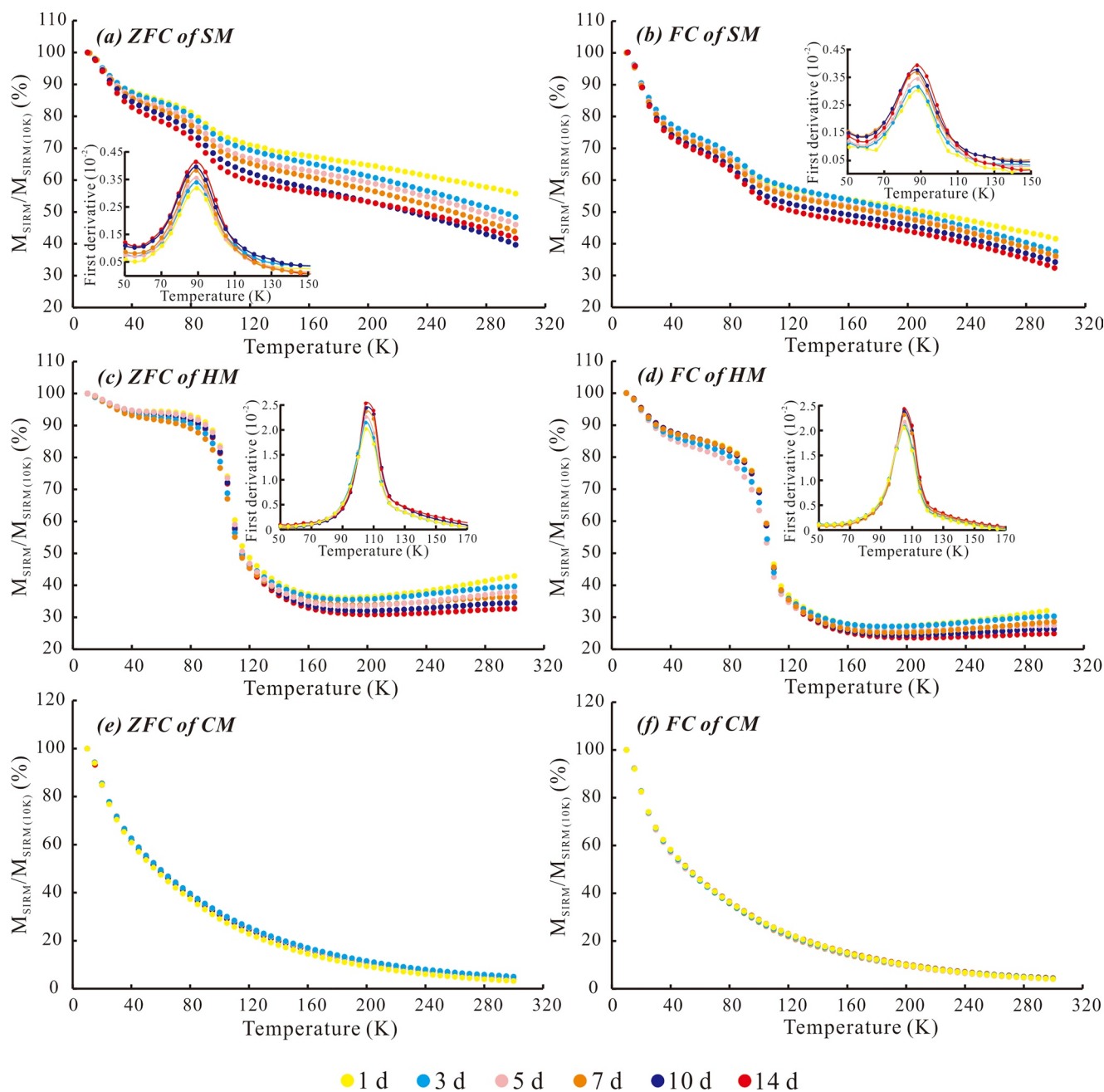


Figure 5. Zero-field warming curves (ZFC, 10–300 K) and field warming curves (FC, 10–300 K) of LT-SIRM of bio-reduced magnetite nanoparticles with different cultivation time. The first derivative curves of zero-field warming curves and field warming curves near Verwey transition region are also shown.

4. Discussion

4.1. Changes in Crystallinity of Magnetite NPs as a Result of Microbial Iron Reduction

Our experiments demonstrated that microbial iron reduction could result in the increases in the lattice constants and the interplanar spacing of magnetite NPs. These changes were ascribed to the reduction of Fe^{3+} in the B site (i.e., octahedrally coordinated Fe^{3+}) (Jiang et al., 2016; Y. L. Li et al., 2009; Porsch et al., 2010). It has been reported that the Fe(III) site occupancy in magnetite plays a vital role in its lattice constants. Gorski and Scherer (2010) showed that the incorporation of excess Fe^{3+} ions into the B site of magnetite would cause a decrease of lattice constants, due to the smaller Goldschmidt radius of Fe^{3+} than that of Fe^{2+} (0.785 Å vs.

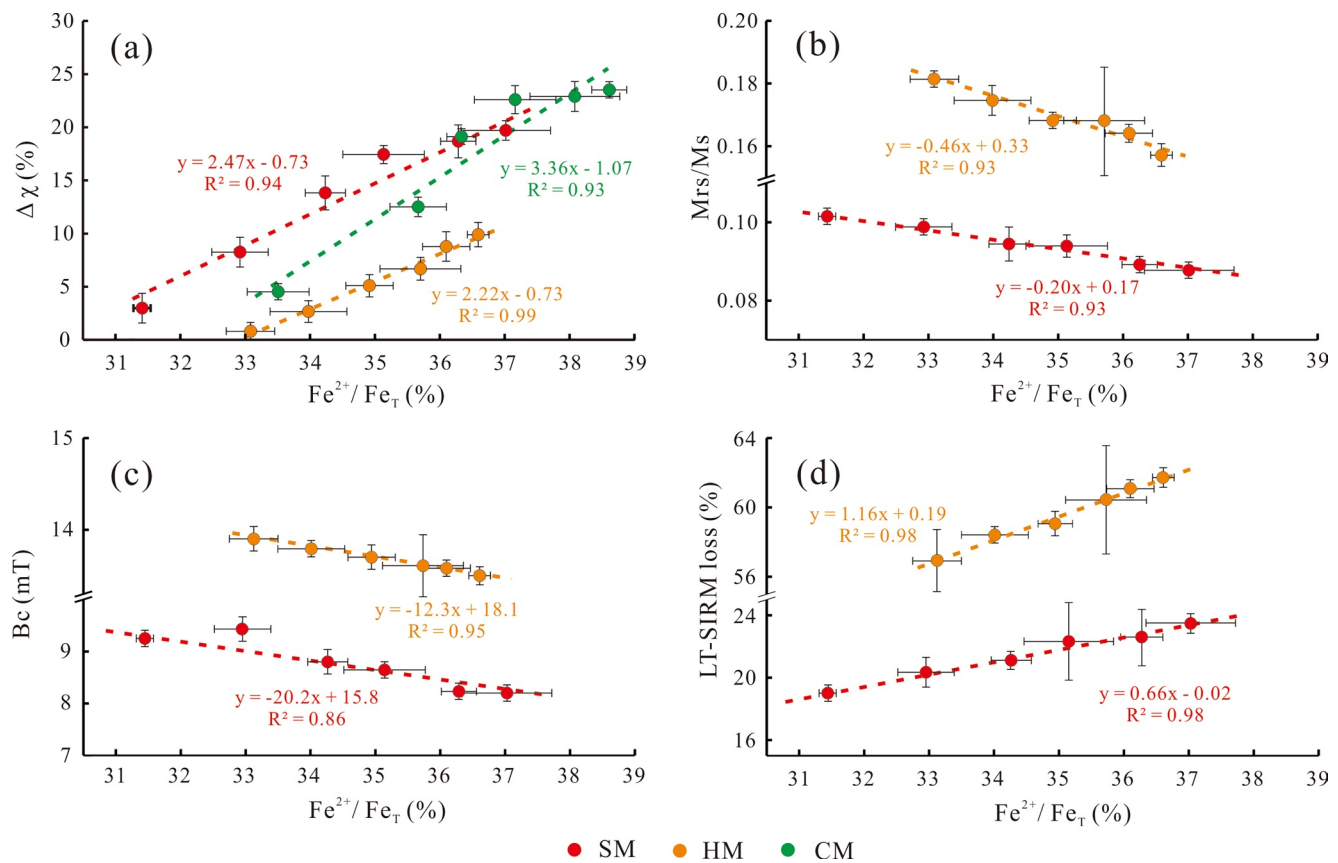


Figure 6. The linear fit of (a) the change of χ ($\Delta\chi$), (b) M_{rs}/M_s , (c) B_c , and (d) LT-SIRM loss near Verwey transition with the Fe^{2+}/Fe_T ratio of magnetite nanoparticles.

0.920 Å). Conversely, the replacement of Fe^{3+} by Fe^{2+} in the B site via an abiotic reduction leads to an increase of lattice constants (Shannon, 1976). It is relevant to note that aforementioned abiotically reduced magnetites still had the Fe^{2+}/Fe_T ratio lower than or equal to 33% (Özdemir & Dunlop, 2010).

Specifically for bioreduction, the Fe^{2+}/Fe_T values of magnetite NPs can be achieved above 33% with strain MR-1 (Table 1). A previous study by Byrne et al. (2016) has demonstrated that the Fe^{3+} on A site is too stable to be accessible to microbial reduction. Therefore, MR-1 cells usually utilize the Fe^{3+} ions on B site as the electron acceptor during bioreduction, which were subsequently reduced to Fe^{2+} ions (Byrne et al., 2015, 2016). In this situation, the excessive Fe^{2+} in B site of magnetite may increase the lattice parameters (lattice constants and interplanar spacing) and lattice defects. As the bioreduction degree increases further, there should be no sufficient sites to accommodate bio-produced Fe^{2+} ions in B site of magnetite, thus leading to an overflow of Fe^{2+} ions released from its lattice (Jiang et al., 2016). It has been proposed that the released Fe^{2+} ions preferentially bound to organic matter (OM), leading to form OM- Fe^{2+} complexes, and adhere onto the magnetite surfaces (Chang et al., 2016; Y. L. Li et al., 2009; Liu et al., 2012; Radon et al., 2020). Such hypothesis was supported by our FTIR results showing the occurrence of organic-magnetite complex (Figure 3). Although dissolved Fe from magnetite NPs (i.e., soluble Fe) was detectable in our bioreactors (0.53–0.99 mM at day 14) (Table 1 and Figure 1b), the fraction of this soluble phase to magnetite-bound Fe was found below 0.21%, which suggests that most of the produced Fe(II) was either structurally coordinated within magnetite or adsorbed by magnetite surfaces. The occurrence of OM- Fe^{2+} complexes as indicated by our FTIR data could provide an alternative mechanism of the stabilization of magnetite-sorbed Fe(II). However, quantitative experiments are warranted to determine the extent and the coordination environment of OM- Fe^{2+} complexes in future studies.

Our study also found that SM was more resistant to bioreduction than HM and CM (Table 1 and Figure 1b). Compared with the other types of magnetite, SM apparently had a lower surface area to volume ratio, thereby providing less reactive sites for MR-1 cells (Byrne et al., 2016). Unlike HM and CM which were highly pure,

SM contained minor maghemite and its crystals were also coated with a corona-like structure (Figure 2a and Figure S1 in Supporting Information S1). Noticeably, no lattice fringes were detected for the corona by HRTEM (Figure 2a), indicating that this corona-like structure was amorphous and probably consisted of ferrihydrite (the amorphous iron hydroxide). Both maghemite and amorphous iron (hydr-) oxide are more susceptible to microbial reduction than magnetite (O'Loughlin et al., 2013). These Fe(III) phases might compete with SM particles for accepting extracellular electrons, thus hindering the reduction of SM. Indeed, maghemite disappeared and the amorphous iron oxide layer became much thinner upon microbial iron reduction (Figure 2 and Figure S1 in Supporting Information S1), indicating these impurities were involved in the bioreduction.

4.2. Changes in Magnetic Parameter of Magnetite NPs as a Result of Microbial Iron Reduction

As shown in Table 1, the M_{rs}/M_s values of SM and HM NPs were lower than 0.2, indicating that the magnetic parameters of these two magnetite NPs are mainly controlled by the pseudo single domain (PSD > 100 nm, $M_{rs}/M_s < 0.5$) (Liu et al., 2012). However, the particle size analyses showed that the mean size was 120 nm for SM and 79.7 nm for HM, respectively (Figures 2a and 2e). These results suggest that both SM and HM contained single domain particles (SD, 20–80 nm) (Jiang et al., 2018; Liu et al., 2012). The proportion of SD particle in HM (~70%, Figure 2e) was significantly higher than that in SM (~30%, Figure 2a), resulting the higher M_{rs}/M_s and B_c values observed in HM (Liu et al., 2012; Özdemir et al., 2002). In addition, CM had a similar particle size to the superparamagnetic particles (SP < 25 nm), and thus displayed the lowest M_{rs}/M_s and B_c values. As a sensitive index to reflect the relative concentration of SP in the samples (Jiang et al., 2018), $\chi_{rd}\%$ showed the highest value in CM among the three magnetite NPs (~6%, Figure 4b). Meanwhile, for SP particle (e.g., CM used herein), 25% of the ions (Fe^{3+} included) are distributed on its surface, much higher than SD and PSD particle (<2.5%), indicating that the surface area to volume ratio of SP particle is higher than that of SD and PSD particle (Y. L. Li et al., 2009; Navrotsky, 2000). Therefore, the CM-Fe(III) was most accessible to MR-1 cells, which can also account for the highest bioreduction rate observed in the CM systems (Table 1 and Figure 1a).

As mentioned earlier, with the increasing bioreduction extents, the Fe^{2+} ions released from magnetite were mostly bound to microbially derived OM, leading to form OM- Fe^{2+} complexes (Chang et al., 2016; Y. L. Li et al., 2009; Liu et al., 2012; Radon et al., 2020). This “passivation” effect of OM can significantly reduce the catalytic activity of magnetite NPs but improve their electrical conductivity (Radon et al., 2020). More importantly, OM- Fe^{2+} complex can also influence the magnetic properties of magnetite (Radon et al., 2020). Compared to magnetite NPs, OM- Fe^{2+} complex has much smaller size (Radon et al., 2020), which can result in the superparamagnetic properties when it is magnetized by external magnetic field (Liu et al., 2012). Therefore, the $\Delta\chi$ of magnetite NPs increased with the elevated reduction extent (Figure 6a). Moreover, because of its smallest particle size, the $\Delta\chi$ of CM was most easily affected by OM- Fe^{2+} complex, causing a larger slope than that of SM and HM (Figure 6a). Previous studies have shown that M_{rs}/M_s can reflect the remanence recording capacity of magnetite, and B_c indicates the difficulty of magnetite affected by external magnetic field (higher B_c indicates “harder” magnetism, on the contrary, indicates “softer” magnetism) (Dunlop, 2002a, 2002b; Liu et al., 2012). For bioreduced magnetite NPs, a part of Fe^{2+} ions could be released from the lattice of magnetite and subsequently attached to the surface of magnetite NPs in the form of OM- Fe^{2+} , causing looser crystal structure, lower internal stability, more lattice defects, and higher SP. That is, the magnetism of bioreduced magnetite is “softer” than the pristine one, corresponding to the lower M_{rs}/M_s and B_c (Figures 6b and 6c). The directional magnetic moments in magnetite NPs will be disturbed with the enhanced atomic thermal motion (Liu et al., 2012). Thus, the remanence recorded by magnetite magnetized at low temperature would decrease with the increase of temperature, especially near the Verwey transition region (Dunlop & Özdemir, 1997; Jiang et al., 2016; Liu et al., 2012; Özdemir & Dunlop, 2010). Because of the “softer” magnetism, there will be a more intense atomic thermal motion in bioreduced magnetite NPs than that in the pristine ones at the same temperature rise. Therefore, during the whole region (10–300 K) and (or) Verwey transition region, the LT-SIRM loss of magnetite NPs with high degree of bioreduction was greater than that of the pristine one and the ones exposed to less bioreduction (Figure 6d).

4.3. Geological and Environmental Implications

Our study showed that microbial iron reduction can influence both the crystallographic and magnetic properties of the magnetite NPs even without changing their mineral types, and particle size and concentration (Byrne et al., 2015; Zhou et al., 2019). Therefore, the bioreduction of magnetite NPs deserves attention when

the magnetic signals are used in paleoenvironment reconstruction (Byrne et al., 2015; Maher, 2009; Mewafy et al., 2011; Zhou et al., 2019).

According to previous studies, oxygen, nitrate and sulphate are unlikely to be present in quantities sufficient to support globally significant rates of microbial metabolism in the pre-Proterozoic (≥ 2.5 Ga) (Vargas et al., 1998; Walker & Brimblecombe, 1985; Wiechert, 2002). Given the facts that solar UV radiation in Archean was significantly stronger than present and free Fe^{3+} ions in seawater can be generated from the UV photooxidation of Fe^{2+} , Fe^{3+} has been thought to be crucial for microbial respiration on early Earth (Vargas et al., 1998; Walker, 1987). Moreover, these free Fe^{3+} ions transform into Fe(III)-bearing minerals (e.g., magnetite) under the combined actions of physics, chemistry and biology in the post sedimentary environment (Y. L. Li, et al., 2013). Magnetite is one of abundant components of banded iron formations, the chemical sedimentary rocks during the Archean and early Proterozoic (~ 3.8 – 1.8 Ga) (Y. L. Li, et al., 2013). Since magnetite has the capability to store up to 2.6×10^{21} electrons/g (Byrne et al., 2015), it is reasonable to speculate that magnetite NPs might be an effective electron sink for microbial respiration in Archean. In the present study, we employed a non-growth iron-reducing system (lacking vitamins and additional organic substrates except lactate) to simulate the oligotrophic conditions of Archean oceans and some modern ecosystems, such as intertidal zone and deep sea (Byrne et al., 2015; Vargas et al., 1998; Wiechert, 2002). Our study, together with others, highlights the importance of magnetite NPs in sustaining DIRB in these environments. In addition, magnetite has been considered as a host for various trace metals (e.g., Ni, Co, V, and Ti) (Han et al., 2021). The interaction between DIRB and magnetite NPs may also affect the cycling of trace metals in Archean oceans. However, future experimental studies are warranted to examine such possibilities.

For the advantages of effective, cheap, and recyclable, magnetite NPs have been widely used in the field of pollutant treatment (Gorski et al., 2010; McCormick & Adriaens, 2004; Radon et al., 2020). The reactivity of magnetite with contaminants is directly linked to the proportion of Fe^{2+} ions in magnetite (Radon et al., 2020). However, magnetite NPs are easily oxidized by air due to their nano-size and highly reactive surface, and then decrease their catalytic activity (Radon et al., 2020). Therefore, in order to prevent the oxidation and maintain the catalytic activity of magnetite NPs, surface modification has been suggested as an effective treatment (Radon et al., 2020). Our study indicated that microbial iron reduction may be an effective approach to the magnetite surface modification by remarkable increasing the structural $\text{Fe}^{2+}/\text{Fe}_T$ ratio and keeping the initial crystal shape and size.

5. Conclusions

In this study, three kinds of magnetite NPs were selected for microbial iron reduction experiments under non-growth conditions. Our results found that all three magnetite NPs can act as electron acceptor for DIRB. The microbial iron reduction could affect the mineralogical and magnetic properties of the magnetite NPs. After bioreduction, the $\text{Fe}^{2+}/\text{Fe}_T$ ratios of magnetite NPs elevated; the lattice parameters and χ of magnetite NPs increased, while the M_{rs}/M_s values and B_c decreased. Compared with more stoichiometric HM and CM, partially oxidized SM was more resistant to bioreduction. The interaction between DIRB and magnetite may be an important post-depositional process in Archean oceans and modern oligotrophic environments, which is overlooked in the reconstruction of paleoenvironment and the study of biogeochemical cycling.

Data Availability Statement

The raw data files (XRD, FTIR, ZFC, and FC) have been deposited in Dryad under reference number: <https://datadryad.org/stash/share/dHacWX4vu249DxkvjAOxUaRie-zpo2Rc8FkmDye1OA>

References

- An, Z. S., & Porter, S. C. (1997). Millennial-scale climatic oscillations during the last interglaciation in central China. *Geology*, 25(7), 603–606. [https://doi.org/10.1130/0091-7613\(1997\)025<0603:MSCODT>2.3.CO;2](https://doi.org/10.1130/0091-7613(1997)025<0603:MSCODT>2.3.CO;2)
- Bazylinski, D. A., & Moskowitz, B. M. (1997). Microbial biomineralization of magnetic iron minerals: Microbiology, magnetism and environmental significance. *Geomicrobiology: Interactions Between Microbes and Minerals*, 35, 181–224. <https://doi.org/10.1515/9781501509247-008>
- Byrne, J. M., Klueglein, N., Pearce, C., Rosso, K. M., Appel, E., & Kappler, A. (2015). Redox cycling of Fe (II) and Fe (III) in magnetite by Fe-metabolizing bacteria. *Science*, 347(6229), 1473–1476. <https://doi.org/10.1126/science.aaa4834>
- Byrne, J. M., Van der Laan, G., Figueroa, A. I., Qafoku, O., Wang, C. M., Pearce, C. I., et al. (2016). Size dependent microbial oxidation and reduction of magnetite nano- and micro-particles. *Scientific Reports*, 6, 1–13. <https://doi.org/10.1038/srep30969>

Acknowledgments

This work is financially supported by grants from the National Natural Science Foundation of China (Nos. 41822402 and 41772362), the 111 Project (No. BP0820004), and the Fundamental Research Funds for National Universities, China University of Geosciences (Wuhan). The authors are grateful to Prof. Claudio Faccenna (the editor) and the two anonymous reviewers whose comments improved the quality of this manuscript.

- Canfield, D. E., Thamdrup, B., & Hansen, J. W. (1993). The anaerobic degradation of organic matter in Danish coastal sediments: Iron reduction, manganese reduction, and sulfate reduction. *Geochimica et Cosmochimica Acta*, 57(16), 3867–3883. [https://doi.org/10.1016/0016-7037\(93\)90340-3](https://doi.org/10.1016/0016-7037(93)90340-3)
- Chang, L., Harrison, R. J., Zeng, F., Berndt, T. A., Roberts, A. P., Heslop, D., & Zhao, X. (2018). Coupled microbial bloom and oxygenation decline recorded by magnetofossils during the Palaeocene-Eocene Thermal Maximum. *Nature Communications*, 9, 4007. <https://doi.org/10.1038/s41467-018-06472-y>
- Chang, L., Heslop, D., Roberts, A. P., Rey, D., & Mohamed, K. J. (2016). Discrimination of biogenic and detrital magnetite through a double Verwey transition temperature. *Journal of Geophysical Research: Solid Earth*, 121(1), 3–14. <https://doi.org/10.1002/2015JB012485>
- Ding, Z. L., Derbyshire, E., Yang, S. L., Yu, Z. W., Xiong, S. F., & Liu, T. S. (2002). Stacked 2.6-Ma grain size record from the Chinese loess based on five sections and correlation with the deep-sea $\delta^{18}\text{O}$ record. *Paleoceanography*, 17(3), 5-1–5-21. <https://doi.org/10.1029/2001PA000725>
- Dong, H. L., Fredrickson, J. K., Kennedy, D. W., Zachara, J. M., Kukkadapu, R. K., & Onstott, T. C. (2000). Mineral transformation associated with the microbial reduction of magnetite. *Chemical Geology*, 169(3–4), 299–318. [https://doi.org/10.1016/S0009-2541\(00\)00210-2](https://doi.org/10.1016/S0009-2541(00)00210-2)
- Dunlop, D. J. (2002a). Theory and application of the day plot (M_r/M_s versus H_r/H_c) 1. Theoretical curves and tests using titanomagnetite data. *Journal of Geophysical Research*, 107(B3), 2056. <https://doi.org/10.1029/2001JB000486>
- Dunlop, D. J. (2002b). Theory and application of the day plot (M_r/M_s versus H_r/H_c) 2. Application to data for rocks, sediments, and soils. *Journal of Geophysical Research*, 107(B3), 2057. <https://doi.org/10.1029/2001JB000487>
- Dunlop, D. J., & Özdemir, Ö. (1997). *Rock magnetism, fundamentals and frontiers*. Cambridge University Press. <https://doi.org/10.1017/CBO9780511612794>
- Faivre, D., & Schuler, D. (2008). Magnetotactic bacteria and magnetosomes. *Chemical Reviews*, 108(11), 4875–4898. <https://doi.org/10.1021/cr078258w>
- Ghosh, R., Pradhan, L., Devi, Y. P., Meena, S. S., Tewari, R., Kumar, A., et al. (2011). Induction heating studies of Fe_3O_4 magnetic nanoparticles capped with oleic acid and polyethylene glycol for hyperthermia. *Journal of Materials Chemistry*, 21(35), 13388–13398. <https://doi.org/10.1039/c1jm10092k>
- Gorski, C. A., Nurmi, J. T., Tratnyek, P. G., Hofstetter, T. B., & Scherer, M. M. (2010). Redox behavior of magnetite: Implications for contaminant reduction. *Environmental Science & Technology*, 44(1), 55–60. <https://doi.org/10.1021/es901684d>
- Gorski, C. A., & Scherer, M. M. (2010). Determination of nanoparticulate magnetite stoichiometry by Mossbauer spectroscopy, acidic dissolution, and powder X-ray diffraction: A critical review. *American Mineralogist*, 95(7), 1017–1026. <https://doi.org/10.2138/am.2010.3435>
- Han, X. H., Tomaszewski, E. J., Schoenberg, R., Konhauser, K. O., Amor, M., Pan, Y. X., et al. (2021). Using Zn and Ni behavior during magnetite precipitation in banded iron formations to determine its biological or abiotic origin. *Earth and Planetary Science Letters*, 568, 117052. <https://doi.org/10.1016/j.epsl.2021.117052>
- Heller, F., & Liu, T. S. (1986). Palaeoclimate and sedimentary history from magnetic susceptibility of loess in China. *Geophysical Research Letters*, 13(11), 1169–1172. <https://doi.org/10.1029/GL013i011p01169>
- Jiang, Z. X., Liu, Q. S., Roberts, A. P., Barron, V., Torrent, J., & Zhang, Q. (2018). A new model for transformation of ferrihydrite to hematite in soils and sediments. *Geology*, 46(11), 987–990. <https://doi.org/10.1130/G45386.1>
- Jiang, Z. X., Liu, Q. S., Zhao, X., Roberts, A. P., Heslop, D., Barron, V., et al. (2016). Magnetism of Al-substituted magnetite reduced from Al-hematite. *Journal of Geophysical Research: Solid Earth*, 121(6), 4195–4210. <https://doi.org/10.1002/2016JB012863>
- Kosterov, A. (2003). Low-temperature magnetization and AC susceptibility of magnetite: Effect of thermomagnetic history. *Geophysical Journal International*, 154(1), 58–71. <https://doi.org/10.1046/j.1365-246X.2003.01938.x>
- Kukkadapu, R. K., Zachara, J. M., Fredrickson, J. K., Kennedy, D. W., Dohnalkova, A. C., & McCreedy, D. E. (2005). Ferrous hydroxy carbonate is a stable transformation product of biogenic magnetite. *American Mineralogist*, 90(2–3), 510–515. <https://doi.org/10.2138/am.2005.1727>
- Lei, W., Liu, Y. S., Si, X. D., Xu, J., Du, W. L., Yang, J., et al. (2017). Synthesis and magnetic properties of octahedral Fe_3O_4 via a one-pot hydrothermal route. *Physics Letters A*, 381(4), 314–318. <https://doi.org/10.1016/j.physleta.2016.09.018>
- Li, J. H., Benzerara, K., Bernard, S., & Beyssac, O. (2013). The link between biomineralization and fossilization of bacteria: Insights from field and experimental studies. *Chemical Geology*, 359, 49–69. <https://doi.org/10.1016/j.chemgeo.2013.09.013>
- Li, J. H., Liu, P. Y., Tamaxia, A., Zhang, H., Liu, Y., Wang, J., & Pan, Y. (2021). Diverse intracellular inclusion types within magnetotactic bacteria: Implications for biogeochemical cycling in aquatic environments. *Journal of Geophysical Research: Biogeosciences*, 126(7), e2021JG006310. <https://doi.org/10.1029/2021JG006310>
- Li, J. H., Liu, Y., Liu, S. C., Roberts, A. P., Pan, H. M., Xiao, T. A., et al. (2020). Classification of a complexly mixed magnetic mineral assemblage in Pacific Ocean surface sediment by electron microscopy and supervised magnetic unmixing. *Frontiers of Earth Science*, 8, 609058. <https://doi.org/10.3389/feart.2020.609058>
- Li, Y. L., Konhauser, K. O., Kappler, A., & Hao, X. L. (2013). Experimental low-grade alteration of biogenic magnetite indicates microbial involvement in generation of banded iron formations. *Earth and Planetary Science Letters*, 361, 229–237. <https://doi.org/10.1016/j.epsl.2012.10.025>
- Li, Y. L., Pfiffner, S. M., Dyar, M. D., Vali, H., Konhauser, K. O., Cole, D. R., et al. (2009). Degeneration of biogenic superparamagnetic magnetite. *Geobiology*, 7(1), 25–34. <https://doi.org/10.1111/j.1472-4669.2008.00186.x>
- Liu, Q. S., Roberts, A. P., Larrasoana, J. C., Banerjee, S. K., Guyodo, Y., Tauxe, L., & Zhao, X. (2012). Environmental magnetism: Principles and applications. *Reviews of Geophysics*, 50, RG4002. <https://doi.org/10.1029/2012RG000393>
- Liu, Q. S., Torrent, J., Maher, B. A., Yu, Y. J., Deng, C. L., Zhu, R. X., et al. (2005). Quantifying grain size distribution of pedogenic magnetic particles in Chinese loess and its significance for pedogenesis. *Journal of Geophysical Research*, 110(B11), B11102. <https://doi.org/10.1029/2005JB003726>
- Lovley, D. R., Coates, J. D., Blunt-Harris, E. L., Phillips, E. J. P., & Woodward, J. C. (1996). Humic substances as electron acceptors for microbial respiration. *Nature*, 382(6590), 445–448. <https://doi.org/10.1038/382445a0>
- Maher, B. A. (2009). Rain and dust: Magnetic records of climate and pollution. *Elements*, 5(4), 229–234. <https://doi.org/10.2113/gselements.5.4.229>
- Maher, B. A. (2011). The magnetic properties of Quaternary aeolian dusts and sediments, and their palaeoclimatic significance. *Aeolian Research*, 3(2), 87–144. <https://doi.org/10.1016/j.aeolia.2011.01.005>
- McCormick, M. L., & Adriaens, P. (2004). Carbon tetrachloride transformation on the surface of nanoscale biogenic magnetite particles. *Environmental Science & Technology*, 38(4), 1045–1053. <https://doi.org/10.1021/es030487m>
- Mewafy, F. M., Atekwana, E. A., Werkema, D. D., Slater, L. D., Ntarlagiannis, D., Revil, A., et al. (2011). Magnetic susceptibility as a proxy for investigating microbially mediated iron reduction. *Geophysical Research Letters*, 38, L21402. <https://doi.org/10.1029/2011GL049271>
- Navrotsky, A. (2000). Nanomaterials in the environment, agriculture, and technology (NEAT). *Journal of Nanoparticle Research*, 2(3), 321–323. <https://doi.org/10.1023/A:1010007023813>

- O'Loughlin, E. J., Boyanov, M. I., Flynn, T. M., Gorski, C. A., Hofmann, S. M., McCormick, M. L., et al. (2013). Effect of bound phosphate on the bioreduction of lepidocrocite (γ -FeOOH) and maghemite (γ -Fe₂O₃) and formation of secondary minerals. *Environmental Science & Technology*, 47(16), 9157–9166. <https://doi.org/10.1021/es400627j>
- Özdemir, Ö., & Dunlop, D. J. (2010). Hallmarks of maghemitization in low-temperature remanence cycling of partially oxidized magnetite nanoparticles. *Journal of Geophysical Research*, 115, B02101. <https://doi.org/10.1029/2009JB006756>
- Özdemir, Ö., Dunlop, D. J., & Moskowitz, B. M. (2002). Changes in remanence, coercivity and domain state at low temperature in magnetite. *Earth and Planetary Science Letters*, 194(3–4), 343–358. [https://doi.org/10.1016/S0012-821X\(01\)00562-3](https://doi.org/10.1016/S0012-821X(01)00562-3)
- Porsch, K., Dippon, U., Rijal, M. L., Appel, E., & Kappler, A. (2010). In-situ magnetic susceptibility measurements as a tool to follow geomicrobiological transformation of Fe minerals. *Environmental Science & Technology*, 44(10), 3846–3852. <https://doi.org/10.1021/es903954u>
- Radon, A., Lonski, S., Kadziolka-Gawel, M., Gebara, P., Lis, M., Lukowicz, D., et al. (2020). Influence of magnetite nanoparticles surface dissolution, stabilization and functionalization by malonic acid on the catalytic activity, magnetic and electrical properties. *Colloids and Surfaces A: Physicochemical and Engineering Aspects*, 607, 125446. <https://doi.org/10.1016/j.colsurfa.2020.125446>
- Shannon, R. D. (1976). Revised effective ionic radii and systematic studies of interatomic distances in halides and chalcogenides. *Acta Crystallographica Section A*, A32, 751–767. <https://doi.org/10.1107/S0567739476001551>
- Tamura, H., Goto, K., Yotsuyanagi, T., & Nagayama, M. J. T. (1974). Spectrophotometric determination of iron(II) with 1,10-phenanthroline in the presence of large amounts of iron(III). *Talanta*, 21(4), 314–318. [https://doi.org/10.1016/0039-9140\(74\)80012-3](https://doi.org/10.1016/0039-9140(74)80012-3)
- Tang, W. S., Su, Y., Li, Q., Gao, S. A., & Shang, J. K. (2013). Superparamagnetic magnesium ferrite nanoadsorbent for effective arsenic (III, V) removal and easy magnetic separation. *Water Research*, 47(11), 3624–3634. <https://doi.org/10.1016/j.watres.2013.04.023>
- Vargas, M., Kashefi, K., Blunt-Harris, E. L., & Lovley, D. R. (1998). Microbiological evidence for Fe (III) reduction on early Earth. *Nature*, 395(6697), 65–67. <https://doi.org/10.1038/25720>
- Walker, J. C. G. (1987). Was the Archaean biosphere upside down? *Nature*, 329(6141), 710–712. <https://doi.org/10.1038/329710a0>
- Walker, J. C. G., & Brimblecombe, P. (1985). Iron and sulfur in the pre-biologic ocean. *Precambrian Research*, 28(3–4), 205–222. [https://doi.org/10.1016/0301-9268\(85\)90031-2](https://doi.org/10.1016/0301-9268(85)90031-2)
- Wiechert, U. H. (2002). Earth's early atmosphere. *Science*, 298(5602), 2341–2342. <https://doi.org/10.1126/science.1079894>
- Zhou, Y. F., Gao, Y., Xie, Q. Q., Wang, J., Yue, Z. B., Wei, L., et al. (2019). Reduction and transformation of nanomagnetite and nanomaghemite by a sulfate-reducing bacterium. *Geochimica et Cosmochimica Acta*, 256(66–81), 66–81. <https://doi.org/10.1016/j.gca.2019.02.040>
- Zhu, Z. M., Han, Z. X., Bi, X. Y., & Yang, W. L. (2012). The relationship between magnetic parameters and heavy metal contents of indoor dust in e-waste recycling impacted area, Southeast China. *The Science of the Total Environment*, 433, 302–308. <https://doi.org/10.1016/j.scitotenv.2012.06.067>